Migratory CO Insertion and Aldehyde Formation in Carbonylation of Methane by the $Rh(PH_3)_2Cl$ Catalyst. A Dynamical Density Functional Study

Peter Margl,[†] Tom Ziegler,*[,†] and Peter E. Blöchl[‡]

Contribution from the Department of Chemistry, University of Calgary, 2500 University Drive N.W., T2N 1N4 Calgary, Alberta, Canada, and IBM Research Division, Zurich Research Laboratory, CH-8803 Rüschlikon, Switzerland

Received December 11, 1995. Revised Manuscript Received March 7, 1996[⊗]

Abstract: Sakakura and Tanaka have recently developed an alkane carbonylation process with the Vaska type complex $Rh(PR_3)_2Cl(CO)$ (**1**) as the (pre)catalyst. We have previously studied the initial steps of the alkane carbonylation process involving C−H activation. Here, we present density functional calculations on the remaining part of the catalytic cycle. This part involves migratory insertion of CO into the Rh−CH_3 bond of $Rh(PH_3)_2Cl(H)(CH_3)(CO)$ (**6**), generating the rhodium acyl $Rh(PH_3)_2Cl(H)(CH_3CO)$ (**11**), and further the addition of another CO molecule to **11**, yielding $Rh(PH_3)_2Cl(CO)(H)(CH_3CO)$ (**12**). Finally, acetaldehyde is eliminated from **12** to regenerate **1**. The present investigation combines "static" calculations of the stationary points on the potential surface with first principles molecular dynamics calculations based on the Car-Parrinello-Projector-Augmented-Wave method. We find that the rate limiting step in the carbonylation of methane is the migratory insertion of coordinated CO into the Rh−CH_3 bond, **6** → **11**, with a barrier of 129 (trans) and 114 kJ/mol (cis), respectively, whereas the reductive elimination of methane from **6** has a lower calculated barrier of 72 (trans) and 57 kJ/mol (cis) according to our previous work. Therefore, the carbonylation will be seriously retarded by the concurrent reductive alkane elimination. We find that the overall productivity of the methane carbonylation process is determined by the migratory insertion step.

1. Introduction

Catalytic activation and subsequent functionalization of the hydrocarbon C−H bond is a continual challenge to organometallic chemistry due to its potential technological impact. Since the pioneering initial steps of Bergman,[1a] Graham,[1b] and Jones,[1c] several new transition metal species capable of activating alkane C−H bonds at or below room temperature have been discovered by a number of groups. It is generally accepted[1−3] that iridium and rhodium-based systems are among the best suited for activating a C−H bond.

Following the early work on C−H activation,[1,2] which was concerned with the basic reaction in which a C−H bond is broken, Sakakura and Tanaka[4] developed complete catalytic cycles for C−H bond functionalizations involving carbonylation, isonitrile insertion C═C double bond insertion, etc. The functionalizaitons are all based on rhodium catalysts activated by photolysis. The complete cycle for the carbonylation of methane is shown in Figure 1.

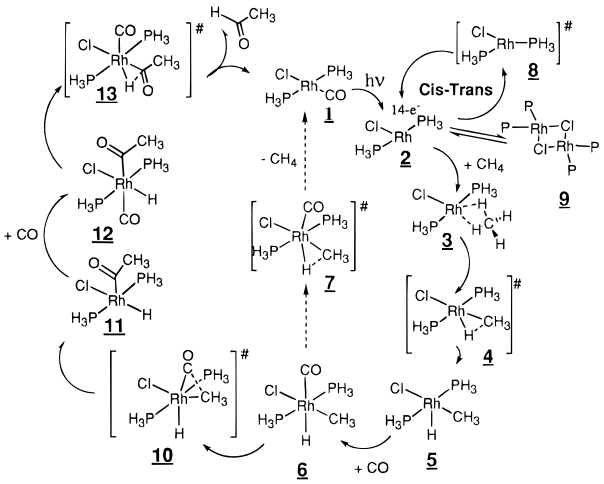

Figure 1. Catalytic cycle for the carbonylation of methane with $Rh(PH_3)_2Cl$. The stages of the reaction are indicated with numbers (**1**−**13**).

The C−H activation steps **2** + CH_4 → **3** → **5** of Figure 1 have already been investigated in a number of studies.[3c,e−g] Our previous work[3g] showed that the elimination of methane **6** → (**7**) → **1** + CH_4, which short-circuits the catalytic cycle, is relatively facile. Also, dimerization of **2** was shown to reduce the amount of active catalyst. Therefore, the overall efficiency of the catalytic carbonylation will crucially depend on the energetics of the productive part of the cycle. In the present work, we carry out an analysis of the productive part of the catalytic cycle **6** → **11** → **12** → **1** + CH_3CHO shown in Figure 1 by using static and dynamic methods based on density functional theory[5] (DFT).

Conventional DFT is a reliable tool in studies of elementary reaction steps.[6] It affords essentially a static view of chemical reactions, usually providing minimum energy paths on the

[†] University of Calgary.
[‡] Zurich Research Laboratory.
[⊗] Abstract published in *Advance ACS Abstracts,* May 15, 1996.

(1) (a) Janowicz, A. H.; Bergman, R. G. *J. Am. Chem. Soc.* **1982**, *104*, 352. (b) Hoyano, J. K.; Graham, W. A. G. *J. Am. Chem. Soc.* **1982**, *104*, 3724. (c) Jones, W. D.; Feher, F. J. *J. Am. Chem. Soc.* **1982**, *104*, 4240.
(2) (a) Crabtree, R. H. *Chem. Rev.* **1985**, *85*, 245. (b) Jones, W. D.; Feher, F. J. *Acc. Chem. Res.* **1989**, *22*, 91.
(3) (a) Low, J. J.; Goddard, W. A., III *J. Am. Chem. Soc.* **1984**, *106*, 8321. (b) Ziegler, T.; Tschinke, V.; Fan, L.; Becke, A. D. *J. Am. Chem. Soc.* **1989**, *111*, 9177. (c) Koga, N.; Morokuma, K. *J. Phys. Chem.* **1990**, *94*, 5454. (d) Song, J.; Hall, M. B. *Organometallics* **1993**, *12*, 3118. (e) Siegbahn, P. E. M.; Svensson, M. *J. Am. Chem. Soc.* **1994**, *116*, 10124. (f) Blomberg, M. R. A.; Siegbahn, P. E. M.; Svensson, M. *J. Am. Chem. Soc.* **1992**, *114*, 6095. (g) Margl, P.; Ziegler, T.; Blöchl, P. E. *J. Am. Chem. Soc.* **1995**, *117*, 12625.
(4) (a) Sakakura, T.; Tanaka, M. *Chem. Phys. Lett.* **1987**, *249*, 1113. (b) Tanaka, M.; Sakakura, T. In *Advances in Chemistry Series*; Moser, W. R., Slocum, D. W., Eds.; American Chemical Society: Washington, DC, 1992; Vol. 230, pp 181. (c) Sakakura, T.; Sodeyama, T.; Sasaki, K.; Wada, K.; Tanaka, M. *J. Am. Chem. Soc.* **1990**, *112*, 7221.

S0002-7863(95)04168-0 CCC: $12.00

potential energy surface connecting reactant(s), transition state(s), and product(s). In this approach, dynamical aspects and temperature effects can be included by statistical methods after mapping out the potential energy surfaces near the minimum energy paths. However, such a mapping is costly in terms of man hours and computer resources.

A very expedient scheme to study the dynamics of a system within the framework of DFT was proposed by Car and Parrinello (CP), in which the dynamics of a system can be studied from first principles without recourse to precalculated and fitted potential surfaces. However, straightforward molecular dynamics simulations do only explore the regions of phase space which are relevant for chemical reactions if low barriers are involved. For processes with high or even moderate barriers (>30 kJ/mol), the events of interest occur sparsely, if at all. Most of the simulation time is thus spent in the more trivial places in phase space, rendering the simulation computationally costly and inefficient.

We combine in the present study conventional electronic structure calculations with the CP method. This is accomplished by employing a technique based on constrained CP dynamics, where we introduce fictitious dynamics along a chosen reaction coordinate in order to sample the phase space in the vicinity of the transition state. The appropriate reaction coordinate as well as the area around the transition state is determined by conventional electronic structure calculations based on the Amsterdam Density Functional program system[7] (ADF) whereas the CP dynamics is carried out with the projector-augmented-wave method (PAW) due to Blöchl.[8]

2. Computational Details

Stationary points on the potential energy surface were calculated with the program ADF, developed by Baerends *et al*.[9] and vectorized by Ravenek.[10] The numerical integration scheme applied for the calculations was developed by te Velde *et al*.[11] The geometry optimization procedure was based on the method due to Versluis and Ziegler.[12] The electronic configurations of the molecular systems were described by a triple-ζ basis set on rhodium[13] for 4s, 4p, 4d, 5s, and 5p. Double-ζ STO basis sets were used for carbon (2s,2p), hydrogen (1s), phosphorus (3s,3p), chlorine (3s,3p), and oxygen (2s,2p), augmented with a single 3d polarization function except for hydrogen where a 2p function was used. The $1s^2 2s^2 2p^6 3s^2 3d^{10}$ configuration on rhodium, the $1s^2$ shell on carbon and oxygen, and the $1s^2 2s^2 2p^6$ shells on phosphorus and chlorine were assigned to the core and treated within the frozen core approximation.[11] A set of auxiliary[14] s, p, d, f, and g STO functions, centered on all nuclei, was used in order to fit the molecular density and present Coulomb and exchange potentials accurately in each SCF cycle. Energy differences were calculated by including the local exchange-correlation potential by Vosko *et al*.[15] with Becke's[16] nonlocal exchange corrections and Perdew's[17] nonlocal correlation correction. In a number of studies,[6c−f] the accuracy of this level of theory has been proven to be within 5 kcal/mol of the experimental result for bond dissociation energies of second-row transition metal systems. Geometries were optimized including nonlocal corrections. First-order scalar relativistic corrections[18] were added to the total energy, since a perturbative relativistic approach is sufficient for 4d metals. All discussions of bond rearrangements in the present paper are based on qualitative orbital interaction arguments. No symmetry constraints were used. Saddle point determinations were initialized by a linear transit search from reactant to product along an assumed reaction coordinate. In each step along the reaction coordinate all other degrees of freedom were optimized. Frequency calculations were carried out to confirm that the structures thus obtained indeed represented transition states.

All reported molecular dynamics simulations were carried out with the Car-Parrinello-Projector-Augmented-Wave (CP-PAW) code developed by Blöchl.[8] The wave function is expanded in plane waves up to an energy cutoff of 30 Ryd. The frozen-core approximation was applied for the same shells as in the ADF calculations. We use periodic boundary conditions with a 12 Å fcc cell. All simulations were performed using the local density approximation in the parametrization of Perdew and Zunger,[19] with gradient corrections due to Becke[16] and Perdew.[17] Long-range electrostatic interactions between different cells are eliminated using a method developed by Blöchl,[20] which is based on fitting an atom-centered Gaussian charge density to the molecular electronic density. These fit charges are also used to describe charge transfer phenomena occurring in reaction simulations. A time step of 10 au is used, correcting the mass of the nuclei to account for the drag of the electrons[21] in the coupled dynamics integrated with the Verlet[22] algorithm. The temperature of the nuclei is controlled by a Nosé[23] thermostat, which creates a canonical (NVT) ensemble. All simulations were conducted at 300 K. To achieve an evenly distributed thermal excitation, the dynamics were initialized with vibrational eigenvectors taken from ADF calculations, and the nuclei were slowly heated with a sinusoidal pulse to avoid detachment of the electrons from the Born−Oppenheimer surface by abrupt changes in the nuclear velocities. To sample phase space in the vicinity of the transition state, we choose a reaction coordinate (RC) which is kept constrained during the dynamics using SHAKE[24] constraints. It is desirable that the RC has a high projection onto the IRC[25] (intrinsic reaction coordinate). All other degrees of freedom are allowed to evolve naturally in time. By slowly varying the constraint, phase space in the vicinity of the transition state can be sampled dynamically,[26] leading to undisturbed dynamics for all motions which are orthogonal to the RC, and to fictitious dynamics along the RC. This makes it possible to investigate even high-lying transition states, such as those encountered in the present study. This method yields information similar to an IRC calculation, except that it is more versatile: it provides information about movements orthogonal to the IRC, without making assumptions about the curvature of the potential surface (i.e. no harmonic approximation).

(5) (a) Parr, R. G.; Yang, W. *Density Functional Theory of Atoms and Molecules*; Oxford University Press: New York, 1989. (b) Ziegler, T. *Chem. Rev.* **1991**, *91*, 651.

(6) (a) *Theoretical Aspects of Homogeneous Catalysis*; van Leeuwen, P. W. N. M., Morokuma, K., van Lenthe, J. H., Eds.; Kluwer Academic Publishers: Dordrecht, The Netherlands, 1995. (b) Koga, N.; Morokuma, K. *Chem. Rev.* **1991**, *91*, 823. (c) Folga, E.; Ziegler, T. *J. Am. Chem. Soc.* **1993**, *115*, 5169. (d) Ziegler, T.; Li, J. *Can. J. Chem.* **1994**, *72*, 783. (e) Li, J.; Schreckenbach, G.; Ziegler, T. *J. Phys. Chem.* **1994**, *98*, 4838. (f) Li, J.; Schreckenbach, G.; Ziegler, T. *J. Am. Chem. Soc.* **1995**, *117*, 486.

(7) ADF version 1.1.3.

(8) Blöchl, P. E. *Phys. Rev. B* **1994**, *50*, 17953.

(9) (a) Baerends, E. J.; Ellis, D. E.; Ros, P. *Chem. Phys.* **1973**, *2*, 41. (b) Baerends, E. J. Ph.D. Thesis, Vrije Universiteit, Amsterdam, 1975.

(10) Ravenek, W. In *Algorithms and Applications on Vector and Parallel Computers*; te Riele, H. J. J., Dekker, Th. J., van de Horst, H. A., Eds.; Elsevier, Amsterdam, 1987.

(11) (a) Boerrigter, P. M.; te Velde, G.; Baerends, E. J. *Int. J. Quantum Chem.* **1988**, *33*, 87. (b) te Velde, G.; Baerends, E. J. *J. Comput. Phys.* **1992**, *99*, 84.

(12) Versluis, L.; Ziegler, T. *J. Chem. Phys.* **1988**, *88*, 322.

(13) (a) Snijders, G. J.; Baerends, E. J.; Vernooijs, P. *At. Nucl. Data Tables* **1982**, *26*, 483. (b) Vernooijs, P.; Snijders, G. J.; Baerends, E. J. *Slater Type Basis Functions for the whole Periodic System*; Internal Report, Free University of Amsterdam, The Netherlands, 1981.

(14) Krijn, J.; Baerends, E. J. *Fit functions in the HFS method*; Internal Report (in Dutch), Free University of Amsterdam, The Netherlands, 1984.

(15) Vosko, S. H.; Wilk, L.; Nusair, M. *Can J. Phys.* **1990**, *58*, 1200.

(16) Becke, A. D. *Phys. Rev. A* **1988**, *38*, 3098.

(17) Perdew, J. P. *Phys. Rev. B* **1986**, *33*, 8822; 34, 7406.

(18) (a) Snijders, J. G.; Baerends, E. J. *Mol. Phys.* **1978**, *36*, 1789. (b) Snijders, J. G.; Baerends, E. J.; Ros, P. *Mol. Phys.* **1979**, *38*, 1909. (c) Ziegler, T.; Tschinke, V.; Baerends, E. J.; Snijders, J. G.; Ravenek, W. *J. Phys. Chem.* **1989**, *93*, 3050.

(19) Perdew, J. P.; Zunger, A. *Phys. Rev. B* **1981**, *23*, 5048.

(20) Blöchl, P. E. *J. Chem. Phys.* **1995**, *103*, 7422.

(21) Blöchl, P. E.; Parrinello, M. *Phys. Rev. B* **1992**, *45*, 9413.

(22) Verlet, L. *Phys. Rev.* **1967**, *159*, 98.

(23) (a) Nosé, S. *Mol. Phys.* **1984**, *52*, 255. (b) Hoover, W. G. *Phys. Rev. A* **1985**, *31*, 1695.

(24) Ryckaert, J.-P.; Ciccotti, G.; Berendsen, H. J. *J. Comp. Phys.* **1977**, *23*, 327.

(25) Fukui, K. *Acc. Chem. Res.* **1981**, *14*, 363.

(26) Straatsma, T. P.; Berendsen, H. J. C.; Postma, J. P. M. *J. Chem. Phys.* **1986**, *85*, 6720.

Chart 1

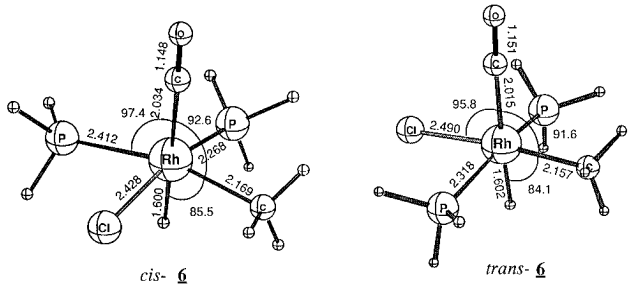

Integrating the force along the reaction coordinate (RC) is a possible way to determine the free energy ΔF of the reaction as $\Delta F = \int_0^1 \langle \partial E/\partial\lambda \rangle|_{\lambda,T}\, d\lambda$, where λ is just the reaction coordinate running between 0, at the beginning of the reaction, and 1, at the end of the reaction. Further, the integrand is the appropriately scaled averaged force on the reaction coordinate sampled at constant temperature and λ. A very convenient way to determine the above integral is to change the reaction coordinate λ continuously from 0 to 1 and to only record one single value of $\delta E/\delta\lambda$ at one given λ. This technique is called "slow growth" method. However, application of this "slow growth" technique to determine ΔF requires a hysteresis curve to be sampled which accounts for the effects of finite RC scan velocity. In practice, only if the chosen RC provides a very large projection upon the true reaction coordinate (IRC) can this technique be successfully applied to free energy calculations. Otherwise, abrupt release of kinetic energy into specific degrees of freedom disturbs the thermal equilibrium, leading to disastrous results for free energy estimates. Additionally, preliminary tests have shown that in order to obtain accurate values for ΔF, the simulation time (currently $\approx$5 ps) must probably be increased by an order of magnitude. We therefore refrain from giving estimates of free energy differences for the reactions discussed here, except for the CO uptake reaction, for which the RC has a high projection upon the true IRC. We will indicate the non-equilibrium character of the ΔF values obtained thus with subscript N (ΔF_N). While thermodynamic integration by the slow growth method for such very short simulations as ours offers no improvement over conventionally (i.e. based on partition functions) derived values, the true virtue of the slow growth method lies in its generality. We exploit this in the present paper by discussing the dynamics perpendicular to the RC, which are not subject to the strict limitations which apply for free energy differences.

3. The Calculation of Stationary Points by Conventional DFT

We shall in this section discuss results from conventional DFT calculations on the migratory insertion of CO into the Rh−CH_3 bond, **6** → **11**, CO uptake, **11** + CO → **12**, and reductive elimination of acetaldehyde, **12** → **1** + CH_3CHO. Methane was taken as a model for alkanes actually functionalized by C−H activation in the studies due to Sakakura and Tanaka.[4] For all calculations PMe_3 was modeled by PH_3. Throughout this paper, we refer to different stages on the reaction coordinate with numbers (**1**−**13**), Figure 1. We shall further specify the substitution pattern of the PH_3 groups by a cis/trans prefix. The steps leading to **6** as well as the unproductive side reactions **6** → (**7**) → **1** and **2** → **9** have been discussed in a previous study,[3g] which has also dealt in detail with the structure and energetics of the different isomers of **6**.

Migratory CO Insertion. The migratory insertion process, *cis*-**6** → *cis*-**11**, has a calculated kinetic barrier of 114 kJ/mol and an exothermicity of −13 kJ/mol, Figure 2. The product *cis*-**11** is shown in Chart 3 and the transition state structure *cis*-**10** in Chart 2. The corresponding *trans*-**6** → *trans*-**11** process has a similar reaction enthalpy of −13 kJ/mol and a slightly higher activation energy of 129 kJ/mol.

Chart 2

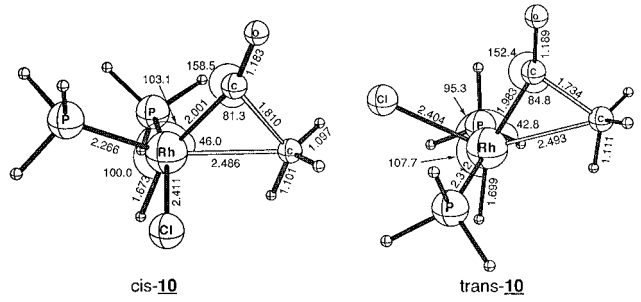

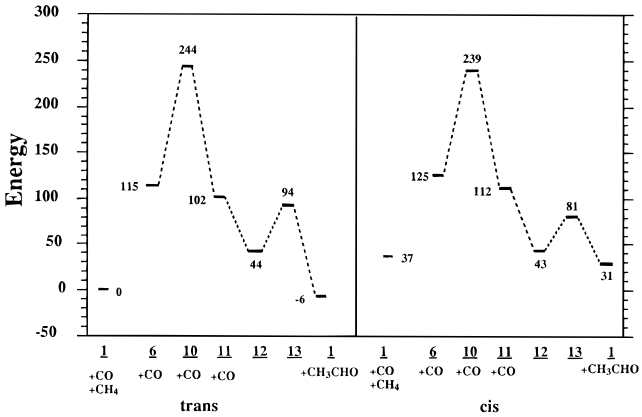

Figure 2. Energy profile for the methane activation, CO uptake, and subsequent elimination of methane. The labels on the *x*-axis refer to different stages of the reaction, as in Figure 1. Energy of free CO was added to that of **6**, **10**, and **11**. Energy of free CH_4 and free CO was added to that of **1** (left). Energy of free CH_3CHO was added to that of **1** (right). Energies are given in kJ/mol, relative to the species *trans*-**1** + CH_4 + CO.

Chart 3

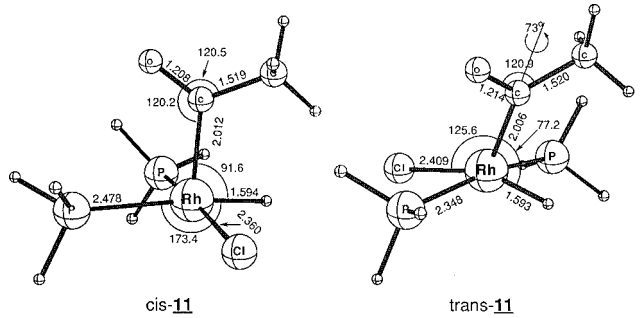

The d^6 products *cis*-**11** and *trans*-**11** are as expected[27] square pyramidal with the acyl group as the stronger π-accepting ligand in the axial position. It is interesting to note that the hydride moves during the reaction from a trans (**6**) to a cis (**11**) position with respect to the carbonyl carbon. This movement takes place after the transition state **10** is reached and ensures that the acyl group occupies its favored apical coordination site.

The migratory insertion involves primarily a single electron pair. On the reactant side (**6**) this pair resides in a σ_{CH_3} orbital stabilized by d_σ on the metal (Figure 3A). Of secondary importance are the three metal centered electron pairs from the d^6 configuration, of which two are residing in d_π orbitals stabilized by π^*_{CO} (Figures 3B and 3C). The corresponding out-of-phase interaction between π^*_{CO} and d_π gives rise to the LUMOs of which one is shown as Figure 3D.

(27) (a) Albright, T. A.; Burdett, J. K.; M. H. Whangbo *Orbital Interactions in Chemistry*; Wiley: New York, 1984. (b) Elian, M.; Hoffmann, R. *Inorg. Chem.* **1975**, *14*, 1058.

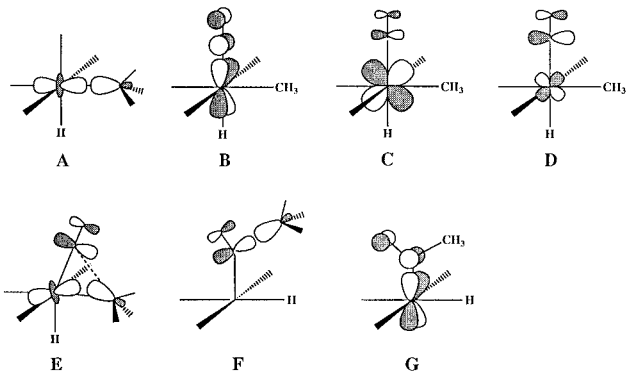

Figure 3. Schematic drawing of molecular orbitals relevant to the migratory insertion of CO into the Rh−CH_3 bond of **6**. For discussion see text.

As the reaction proceeds toward transition state **10**, the electron pair in the σ_{CH_3} orbital becomes destabilized. This is because the methyl group has to reorient its local C_3-axis away from the metal center toward the carbonyl carbon (Figure 3E). This destabilization is a major contributor to the large calculated barrier (Figure 2). The barrier can be reduced to some degree by involvement from the π^*_{CO} based LUMO (Figure 3D), as indicated in Figure 3E. The degree of involvement depends on the energy and composition of the orbital corresponding to Figure 3D. In the present case the d_π to π^*_{CO} interactions (Figures 3B and 3C) are considerable since CO is the only strong π-acceptor. This is manifested in the large calculated[3g] Rh−CO bond dissociation energy of 100 kJ/mol. The consequence of the strong Rh−CO interaction is that the LUMO (Figure 3D) is strongly antibonding with high energy and a less than 100% contribution from π^*_{CO}. Thus, the Rh−CO antibonding orbital of Figure 3D is not well suited to reduce the barrier by lowering the energy of the CH_3 σ orbital (Figure 3E). Of secondary importance is the fact that the electron pair in the d_π orbital of the migration plane (Figure 3C) is destabilized to some degree by the reduction in the d_π to π^*_{CO} overlap as the CO ligand moves toward the methyl group (**10**).

On the product side (**11**) a full interaction is now established between σ_{CH_3} and π^*_{CO} to form the C−C σ-bond on the acyl group (Figure 3F), holding the primary electron pair. One of the secondary electron pairs in a d_π orbital is again stabilized by the interaction between the π^*_{CO} orbital of the carbonyl group and d_π, Figure 3G. However, the other secondary electron pair in the d_π orbital of the migrating plane (Figure 3C) has lost its stabilizing interaction with π^*_{CO} as this orbital becomes involved in the C−C σ-bond on the acyl group. The total energy of *cis*- and *trans*-**11** was found to be largely independent of the rotation of the acetyl group about the Rh−C axis (the angle of 73° in *trans*-**11**, Chart 3, refers to the torsion of the acyl group with respect to the hydride ligand). The maximum variation of the total energy due to this rotation was 5 kJ/mol.

Baird *et al.*[28] have studied the acyl complex $RhCl_2(COR)(PR_3)_2$, which is related to **11** by substitution of a hydride ligand with a chloride ion. They were able to identify species with the phosphines in cis and trans positions analogous to *cis*-**11** and *trans*-**11**, respectively. Also, the trans conformer was found to be the more stable one, just as in the present investigation. Baird *et al.*[28] characterized the trans conformation by X-ray diffraction as a square-pyramidal species with the acyl in an apical position. The observed geometrical parameters for *trans*-$RhCl_2(COR)(PR_3)_2$ are in excellent agreement with those optimized in the case of *trans*-**11** (deviations of bond lengths: Rh−P 0.5%, Rh−Cl 3.1%, Rh−C 3.9%), considering the substitution of a Cl ligand by hydride.

The same authors[28] monitored the decarbonylation of the Rh−Me bond of *trans*-$RhCl_2(COMe)(PR_3)_2$, which leads to the octahedral methyl complex $RhMeCl_2(CO)(PR_3)_2$ in a process similar to *trans*-**11** → *trans*-**6**. They found the acyl−alkyl isomerization reaction to be slightly exothermic by −8 kJ/mol whereas we find the corresponding process *trans*-**11** → *trans*-**6** to be slightly endothermic by the same amount. Thus, both investigations find the acyl complex and its decarbonylation product to be close in energy. Baird *et al.*[28] did not carry out actual kinetic measurements on the decarbonylation reaction. However, they did observe that it took >2 h for *trans*-$RhCl_2(COMe)(PR_3)_2$ to reach equilibrium with $RhMeCl_2(CO)(PR_3)_2$. We can explain this with the high barrier calculated for the decarbonylation reaction, Figure 2. Finally, the authors were considering several possible rearrangements of an acyl complex such as *trans*-**6** in order for the methyl group to end up cis to the CO ligand in the decarbonylation. It follows from the present study that one of the equatorial ligands, in our case the hydride, moves during the last part of the methyl migration so as to end up trans to carbonyl and open a cis position for the migrating methyl group.

The migratory insertion of CO into the Rh−methyl bond of $RhMeCl_2(CO)(PR_3)_2$ is very similar to the well-studied[29,30] CO insertion reaction $CH_3Mn(CO)_5$ → $CH_3C(O)Mn(CO)_4$. The metal center is in both cases six-coordinated with a d^6 electron count. The latter process is characterized by the formation of an acyl group in the basal rather than apical position, whereas the apical site now is occupied by a CO ligand. This arrangement is understandable since CO is a better π-acceptor than the acyl group. Also, the manganese system has a lower calculated activation barrier[31] of 75 kJ/mol. This can be rationalized by observing that the LUMO in $CH_3C(O)Mn(CO)_4$ is analogous to Figure 3D but of lower energy and thus better able to stabilize the transition state in an interaction similar to Figure 3F. The lower orbital energy is a result of a weaker Mn−CO interaction for each individual Mn−CO bond since $CH_3Mn(CO)_5$ contains five competing π-accepting ligands. It follows from the discussion above that the insertion barrier for the process $RhCl(H)(CO)(Me)(PR_3)_2$ → $RhCl(H)(COMe)(PR_3)_2$ might be lowered by using a better π-accepting ligand such as $P(OR)_3$ in place of PR_3.

Reductive Elimination of Acetaldehyde. By uptake of CO into the free octahedral coordination site, **11** transforms into **12** which is the direct precursor for aldehyde elimination. We calculate the exothermicity of CO addition to be −58 kJ/mol (trans) and −69 kJ/mol (cis), respectively. The optimized structures for **12** are shown in Chart 4. It follows from our calculations that the Rh−CO bond in **12** is weaker than in **6** where the Rh−CO dissociation energy was 100 kJ/mol. This is understandable since the acyl group is competing with the CO ligand for electron density in **12**. We note in this regard that the Rh-C_{acyl} bond is 0.1 Å longer in **12** with a CO trans to the acyl group than in **11** with a vacant site trans to the acyl ligand.

The elimination of acetaldehyde proceeds via the transition state **13** shown in Chart 5. The calculated activation energies for **12** → **1** + CH_3CHO are 50 (trans) and 38 kJ/mol (cis), respectively, with an overall exothermicity of −50 (trans) and −12 kJ/mol (cis), respectively. During the elimination, the

(28) Egglestone, D.; Baird, M. C.; Lock, C. L. J.; Turner, G. *J. Chem. Soc., Dalton Trans.* **1977**, 1576.

(29) Boese, W. T.; Ford, P. C. *J. Am. Chem. Soc.* **1995**, *117*, 8381.

(30) Ziegler, T.; Versluis, L.; Tschinke, V. *J. Am. Chem. Soc.* **1986**, *108*, 612.

(31) (a) Versluis, L.; Ziegler, T. *Organometallics* **1990**, *9*, 2985. (b) Sola, M.; Ziegler, T. *Organometallics*. Submitted for publication.

Chart 4

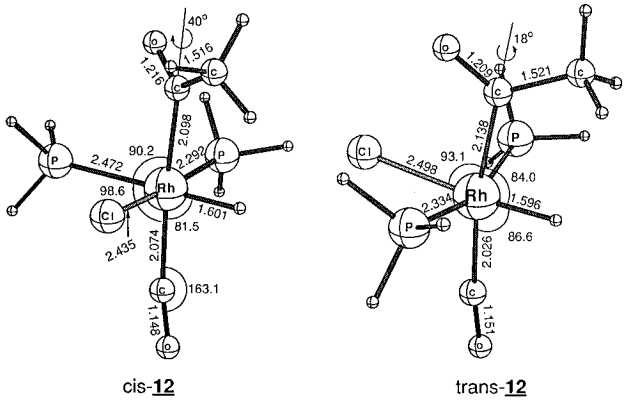

Chart 5

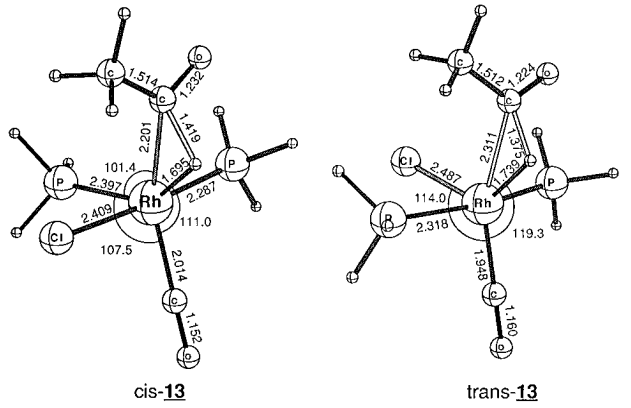

hydride moves toward the carbonyl carbon of the acyl group, maintaining its interaction with the metal center throughout. The transition state **13** can be viewed as an η^2-adduct between the butterfly shaped d^8 fragment $Rh(PH_3)_2(CO)Cl$ and an elongated carbon−hydrogen σ-bond. The transition state **13** is stabilized by donation from the σ_{CH} bond orbital into the LUMO of the fragment $Rh(PH_3)_2(CO)Cl$ and back-donation from the HOMO of $Rh(PH_3)_2(CO)Cl$ into the σ^*_{CH} orbital. We have previously[31] calculated a barrier of only 10 kJ/mol for the aldehyde elimination from $CH_3C(O)Co(H)_2(CO)_3$ in the last step of the catalytic hydroformylation process. The lower barrier reflects the better ability of the CO coligands to accept electron density left behind from the formal reduction of the metal center in the aldehyde elimination. The corresponding complex RhCl(H)-(COMe)$(PR_3)_2$ does not have coligands of the same π-accepting strength. However, it might help to replace the phosphines by $P(OR)_3$ ligands. Alternative pathways for aldehyde elimination are conceivable, f.i. such involving the dissociation of a coligand prior to aldehyde elimination. In the present case, this does not seem practical since the coligands are strongly bound and therefore not prone to dissociation.

4. CP-PAW Molecular Dynamics Simulations

Migratory Insertion of CO into the Rh−CH_3 Bond of *trans*-6. The molecular dynamics simulation was initiated from the ADF structure of *trans*-**6**. The initial velocities were constructed from vibrational eigenvectors of the molecule calculated by ADF. The distance between the methyl carbon and the carbonyl carbon was chosen as reaction coordinate. The corresponding reaction coordinate length (RCL) was decreased over the following 20 000 time steps (≈4.84 ps) from 3.0 to 1.5 Å. This interval brackets the C−C distances of 2.994 and 1.520 Å optimized by ADF for *trans*-**6** and *trans*-**11**, respectively. Changes in important geometrical parameters during the reaction are given in Figure 4, A−C. Figure 4D displays the force on the RC constraint as a function of RCL.

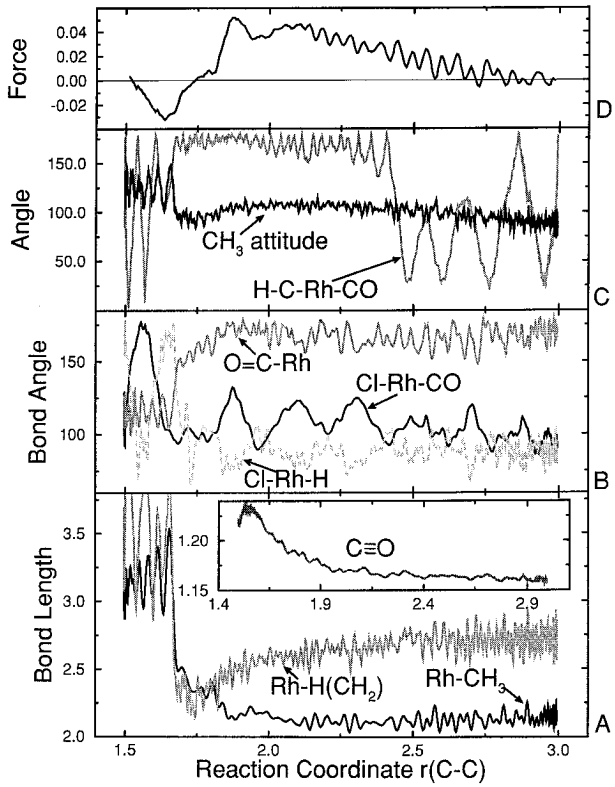

Figure 4. Geometric quantities as functions of the reaction coordinate length (RCL = distance $C_{carbonyl}-C_{methyl}$) during the reaction simulation of the migratory insertion of CO into the Rh−CH_3 bond at 300 K. The reaction *trans*-**6** → *trans*-**11** proceeds from the right-hand side of the graph to the left. (A) Distance between Rh and methyl carbon (dark line, "Rh−CH_3") and between Rh and the methyl hydrogen atom undergoing agostic bonding during methyl migration (gray line, "Rh-$H(CH_2)$"). Insert shows the distance between the carbonyl carbon atom and oxygen. (B) Bond angles. (C) Light line: Torsion angle between the agostic methyl hydrogen, the methyl carbon, the Rh atom, and the carbonyl C atom (H−C−Rh−CO). Solid line: The angle between the methyl C_3 axis and the Rh−CO bond ("CH_3 attitude"). (D) Force on the reaction coordinate (RC). The scanning velocity was determined by a third-order polynomial to avoid abrupt accelerations. This results in a higher number of scan points per RCL unit near the beginning and the end of the simulation. The RC was scanned from 3.0 to 1.5 Å. The horizontal thin lines at zero in (D) correspond to the zero of force. All distances in angstrom units, angles in degrees, force in atomic units.

The initial stages of the migratory insertion process correspond to a bend of the C−Rh−C angle from 90° to 45°, resulting in a contraction of the C−C distance from RCL = 3.0 Å to RCL = 2.1 Å. The actual bond making and bond breaking takes place in the interval RCL = 1.8 to 1.7 Å where the interaction between the two carbons becomes dominant. In this interval the Rh−CH_3 bond is suddenly expanded, Figure 4A, and the C−O distance increases from 1.15 to 1.23 Å (Figure 4A) as density is donated from σ_{CH_3} into the π^*_{CO} orbital according to Figure 3E. The transition state was located by static DFT calculations at RCL = 1.73 Å (*trans*-**10**), which concurs well with the zero point for the force on the RC constraint encountered at ≈1.75 Å RCL, Figure 4D, in the molecular dynamics calculations. The final formation of the stable acyl complex *trans*-**11** takes place at RCL below 1.7 Å.

Changes of the molecular shape are well described by a few characteristic skeletal angles, which are monitored in Figure

4B. The angle of intersection between the C_3 axis of the methyl group and the Rh−CO bond ("CH_3 attitude" in Figure 4B) shows that the methyl group slides along the Rh−CO bond, hardly changing its orientation (initially ≈90°) with respect to the Rh−CO bond until the transition state is surmounted, whereupon the angle drastically increases and oscillates around 120°. The Rh−C−O angle vibrates around the 180° equilibrium value up to the transition state. After this point the angle drops rapidly to 120° (Figure 4B) in concert with the Rh−CH_3 bond rupture (Figure 4A).

The migration of the methyl group is also stabilized by an α-agostic interaction between rhodium and a methyl hydrogen atom in the interval RCL = 2.3 to 1.65 Å around the transition state at RCL = 1.75 Å. Figure 4C reveals that from 3 to 2.5 Å RCL the torsion angle H−C−Rh−CO is variable, indicating that the methyl group is essentially a free rotor at this stage of the reaction. As the three-centered transition state begins to form below 2.5 Å RCL, the rotation freezes, pointing to a directional preference of the methyl group. As soon as the Rh−CH_3 bond is broken, the directional preference again vanishes (below 1.65 Å RCL). It is also possible to follow the agostic interaction by monitoring the Rh−H distance for the methyl hydrogen atom involved (Figure 4A, "Rh−H(CH_2)"). In the first stages of the insertion reaction (RCL = 3−2.5 Å), the Rh−H distance is quite large for an agostic bond (≈2.5 Å), although the rotation becomes arrested already at 2.3 Å RCL. At the transition state, RCL ≈ 1.75 Å, the Rh−H distance is ≈2.25 Å, which is in the range expected for an agostic bond. The methyl group becomes strongly polarized as the reaction approaches the transition state, with the agostic hydrogen bearing a negative charge of ca. −0.1 and the two other hydrogen atoms each bearing ca. +0.1 charges (here −1 corresponds to the charge of an electron). After the transition state has been passed, the CH_3 moiety again becomes a free rotor.

Fluxionality of five-coordinated complexes of this type has already been observed in a previous study.[3g] Fluxional events were also observed in the present migratory insertion reaction. They can be traced through the Cl−Rh−H and Cl−Rh−CO angles, Figure 4B. Following the rupture of the Rh−CH_3 bond at RCL = 1.75 Å, the hydride immediately assumes a position trans to chlorine by a change in the Cl−Rh−H angle from 90° to 180°. This is done in order for hydrogen to avoid the trans influence of the acyl group. The energy which is released into the system by the rupture of the Rh−CH_3 bond also affects the chlorine atom. This atom moves from the trans-hydride to a cis-hydride position (1.55 Å RCL). It returns to the trans-hydride position at 1.51 Å RCL. Several examples[29−31] are known in which the CO double bond of the acyl group binds in a η^2-conformation to the metal center. However, no evidence was found for the formation of such a conformation. The amount of energy released into the acyl group after the Rh−CH_3 bond is broken is considerable[32] and should be sufficient to surmount the barrier between η^1-acyl and η^2-acyl.

The time-dependence of the Coulomb charges on the nuclei is shown in Figure 5. This graph makes it possible to follow processes in which electron density is redistributed between groups within a molecule. Figure 5A reveals that during the migration process electron density is transferred from the methyl group to the acyl oxygen, whereas the carbonyl carbon atom maintains its charge. It would appear from our simple discussion of the C−C σ-bond formation in Figure 3F that charge should be transferred from methyl to the acyl carbon as density

(32) This abrupt release of energy into a few specific degrees of freedom violates thermal equilibrium and is one of the reasons why no free energy differences can be estimated for this particular simulation.

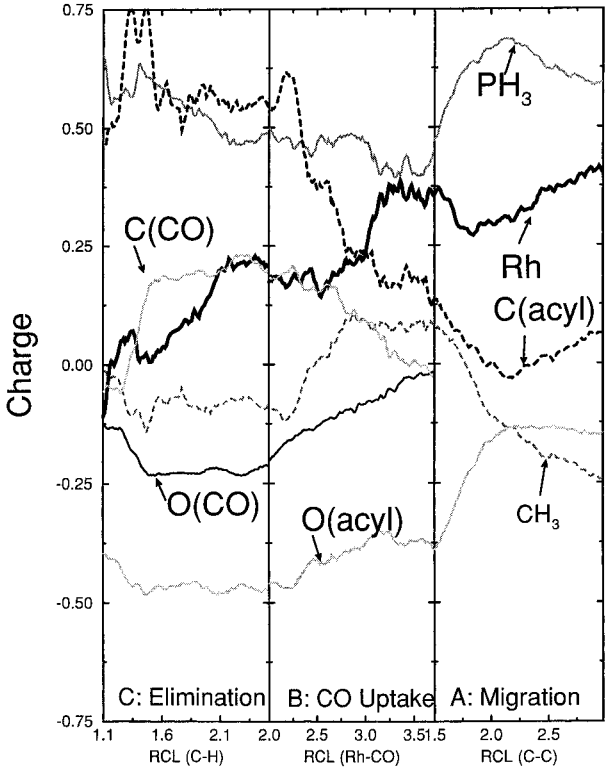

Figure 5. Charges calculated according to ref 20 for the three elementary reaction steps investigated: (A) migratory insertion of CO into the Rh−CH_3 bond of *trans*-**6**; (B) CO uptake of *trans*-**11**; and (C) reductive elimination of CH_3CHO from *trans*-**12**. Read from the right to the left the three graphs correspond to the reaction **6** → (**10**) → **11** + CO → **12** → (**13**) → **1** + CH_3CHO. A charge of −1 corresponds to one electron. Only those functional groups are represented whose charge changes by more than a total of 0.1 units throughout all three reactions. "PH_3": Sum of charges on both phosphine groups. "CH_3": Charge on the methyl group.

is donated from σ_{CH_3} to π^*_{CO}. However, one also has to take into account the electron pair in the corresponding π_{CO} orbital. The density of this pair is shifted toward the oxygen atom to minimize electron−electron repulsion by mixing π_{CO} and π^*_{CO}. The net result is a transfer of charge from methyl to the acyl oxygen atom.

CO Uptake/Dissociation by *trans*-11. The molecular dynamics simulation was initiated from the ADF structure of *trans*-**11**, with the Rh−CO distance chosen a little below its value in the equilibrium structure. For computational convenience CO dissociation instead of uptake was modeled, but since this reaction is entirely reversible the actual choice of direction is irrelevant. Therefore, reading Figure 6 from left to right corresponds to CO dissociation, whereas reading from right to left corresponds to CO uptake. In the following section we will discuss it in terms of the uptake reaction. The initial velocities were constructed from vibrational eigenvectors of the molecule calculated by ADF. The distance between the rhodium atom and the carbonyl C atom was chosen as reaction coordinate. This distance was increased over the following 20 000 time steps (≈4.84 ps) from 1.9 to 3.7 Å. Figure 6 displays changes in important structural data.

Since the CO molecule is a very strong trans ligand, its effect upon the bond length of the trans standing coligand is profound. Figure 6A shows the increase of the Rh−acyl bond length caused by the coordinating CO molecule. For better visibility a fourth-order polynomial fitted to the actual bond length was superimposed. As the CO molecule approaches the metal center, its mobility decreases. The most remarkable change

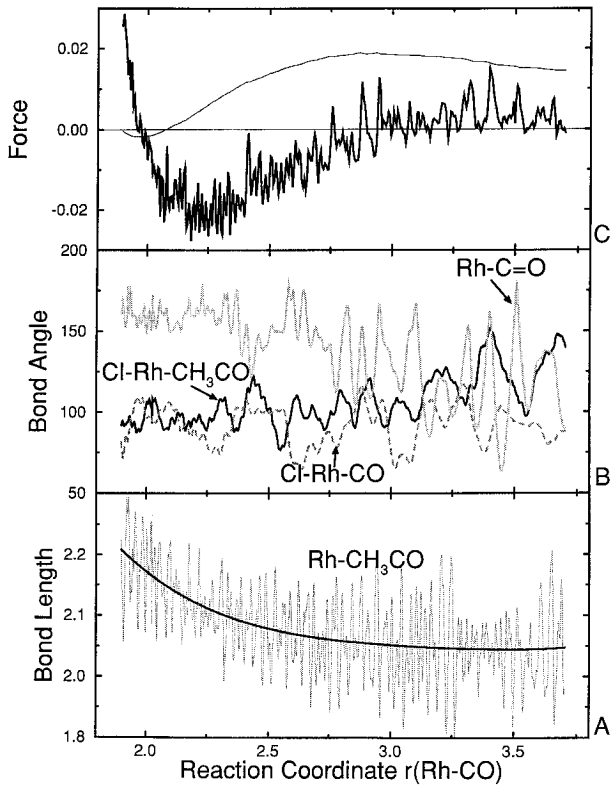

Figure 6. Geometric quantities as a function of the reaction coordinate (RC = Rh−$C_{carbonyl}$ distance) during the simulation of the CO uptake reaction at 300 K. The reaction *trans*-**11** + CO → *trans*-**12** proceeds from the right hand side of the graph to the left. (A) Distance between Rh atom and acyl group. The thick line corresponds to a fourth-order polynomial fit. (B) Skeletal bond angles. (C) Force on the RC (thick line) and its integral $\Delta F_N = \int \delta E/\delta\lambda \, d\lambda$ (thin line). Units as in Figure 4; ΔF_N in atomic units.

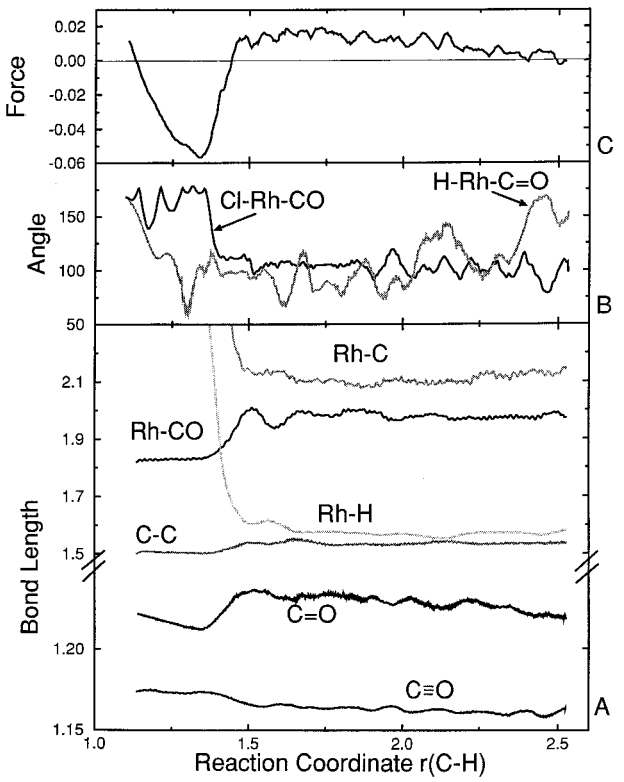

Figure 7. Geometric quantities as a function of the reaction coordinate (RC = hydride−C_{acyl} distance) during the reaction simulation of the reductive elimination of acetaldehyde at 300 K. The reaction *trans*-**12** → *trans*-**1** + CH_3CHO proceeds from the right hand side of the graph to the left. (A) Bond distances. (B) "H−Rh−C=O": Torsion angle between the hydride atom, Rh, and the acyl carbonyl group. "Cl−Rh−CO": Bond angle between Cl, Rh, and the carbonyl moiety which remains at the metal center after aldehyde elimination. (C) Force on the RC. Units as in Figure 4.

happens to the Rh−C−O angle (Figure 6B), which measures how the incoming CO approaches the Rh center (C atom pointing toward the Rh atom: Rh−C−O = 180°; O atom toward Rh: Rh−C−O = 0°). At large values of the RCL, the CO molecule is orientationally not fixed with respect to the metal complex, so that the Rh−C−O angle is variable between 180° and 60°. As the Rh−CO distance is decreased, this angle becomes gradually more rigid until at RCL = 2.0 Å it is confined to the usual mobility of a carbonyl moiety attached to a metal center. At the same time, the Cl−Rh−CO angle (Figure 6B), which measures the extent to which the center-of-mass motion of the CO molecule remains relatively stable, indicates that already at 3.7 Å RCL the CO molecule is trapped by the metal center. *trans*-**11** is strongly distorted from the shape of a square pyramid (Chart 3). This distortion is gradually removed by the incoming CO (Figure 6B, angle Cl−Rh−CH_3CO), so that at the end of the uptake reaction, the angle has assumed its normal octahedral value of 90°.

The force on the RC as given in Figure 6C shows the behavior expected for such a reaction. The force initially increases from zero to slightly positive values as the RC is contracted from 3.7 to 3.25 Å. This is because the van der Waals interaction of the CO with the other ligands becomes unfavorable when the Rh−CO distance is decreased but the Rh−C bond is not yet strong enough to contribute favorably to the overall energy. When the distance is decreased the contribution of the Rh−CO covalent bond becomes dominant and the force becomes negative (below 3.0 Å RCL). Since this chosen reaction coordinate (distance Rh−CO) has a large projection upon the true IRC at all times during the reaction, we can evaluate the free energy differences along the reaction coordinate using the "slow growth" integration.[24,26,33] Based on our unidirectional scan of the RC, this integration scheme yields a free energy of activation $\Delta F_N^{\ddagger} = +11$ kJ/mol and a total exothermicity of $\Delta F_N = -44$ kJ/mol. It it interesting to note that the "slow growth" method is able to determine the free energy of activation in a very simple manner for reactions which do not have an electronic barrier. Evaluating free energy differences for such systems is much less straightforward when one has computed these quantities from molecular partition functions.

The docking process of the CO molecule to the Rh center effects two major redistribution processes of electron density (Figure 5B). Firstly, the carbonyl is polarized during the approach, as seen by the split in the previously very similar charges of carbonyl C and O atoms. The docking process transfers charge from the carbon atom to the oxygen atom. Secondly, the charge density at the central C atom of the acetyl group is depleted, whereas the acylic methyl group and the Rh center gain electron density.

Reductive Elimination of CH_3CHO from *trans*-12. We model the reductive elimination process by starting a molecular dynamics simulation from the ADF structure of *trans*-**12**, using the distance between the acylic carbon and the hydride atom as the reaction coordinate. This distance was decreased over the following 27 500 time steps (≈6.65 ps) from 2.53 to 1.095 Å. Important structural data appear in Figure 7.

Firstly, the effect of acetaldehyde elimination is that the bonds between the remaining ligands and Rh are strengthened as

(33) Margl, P.; Lohrenz, J. C. W.; Ziegler, T.; Blöchl, P. E. *J. Am. Chem. Soc.* **1996**, *118*, 4434.

electron density is donated from the formally reduced metal center to the remaining ligands. This is shown f.i. in Figure 7A for the Rh−CO distance. Secondly, bonds of the second coordination sphere, such as the carbonyl C−O bond (Figure 7A), are weakened due to stronger donation of metal electrons into the π^*_{CO} orbitals. Thirdly, bonds within the ejected aldehyde contract subsequent to elimination as the electron donation from the metal disappears (Figure 7A; C═O, C−C). The actual dissociation of the aldehyde from the metal center at RCL = 1.6−1.2 Å is marked by a steep increase of the Rh−H and Rh−C bond distances as illustrated in Figure 7A.

As the acetaldehyde moiety leaves the metal center, the remaining ligands instantly regroup to form the square-planar Vaska-type complex *trans*-**1**. Correspondingly, the Cl−Rh−CO angle snaps from 100° to 180° at 1.4 Å RCL. In the compound *trans*-**12**, the acetyl moiety is practically a free rotor about the Rh−C axis. As the C−H distance is gradually decreased, we expect the rotor to become stiffer and to assume its proper orientation with respect to the incoming hydrogen atom. The torsion angle H−Rh−C═O in Figure 7B shows that indeed in the earlier stages the acyl moiety rotates quite freely, but becomes fixed at around 100° between 2.0 and 1.4 Å RCL.

The reductive elimination of the aldehyde replinishes electron density at the metal center (Figure 5C). The CO moiety which has been attached during the CO uptake process is depolarized by the formal change of oxidation state at the metal from +3 to +1, with the C atom undergoing the biggest change. The charge to accomplish this is contributed evenly by all other ligands.

5. Concluding Remarks

The present study concludes a full investigation of the alkane carbonylation process developed by Sakakura and Tanaka[4] (Figure 1). The investigation was initiated in a previous study.[3g] It is based on an approach that combines static DFT calculations[5b] with dynamic CP-PAW simulations[8] at 300 K.

We find that the rate limiting step in the carbonylation of methane is the migratory insertion of CO into the Rh−CH_3 bond, **6** → **11**, with a barrier of 129 (trans) and 114 kJ/mol (cis), respectively. The C−H activation, **2** → **5**, is by comparison much more facile with barriers of 14 (trans) and 64 kJ/mol (cis), respectively. Even the reductive elimination of methane from **6** has a lower calculated barrier of 72 (trans) and 57 kJ/mol (cis), respectively. Therefore, the carbonylation will be seriously retarded by the concurrent reductive alkane elimination. Since phosphite ligands are expected to be better π-acceptors than phosphines, it might be possible to facilitate the CO insertion process by replacing the phosphines on the catalyst with more electron accepting phosphite ligands. Unfortunately, such a substitution will at the same time raise the barrier for the C−H activation process, **2** → **5**, and lower the activation energy for the elimination of methane from **6**.

The three-centered mechanism found for migratory insertion is in agreement with previous work.[6,30] In the present case, migratory insertion of CO into the Rh−CH_3 bond entails rearrangement at the metal center. The hydride ligand shifts its position from *cis*-Cl to *trans*-Cl to avoid unfavorable trans interaction with the formed acetyl ligand. Furthermore, the energy release following the formation of the C−C bond causes an intermediary pseudorotation, during which the Cl atom occupies the position trans to the acyl group. Such fluxional phenomena of square-pyramidal complexes have also been observed previously.[3g] In contrast to previous experience for metal acyl complexes,[30] we have found no evidence of η^2-coordination of the acyl carbonyl group. The transition state for migration is stabilized by the formation of a β-agostic bond between a methyl hydrogen atom and rhodium. However, no evidence of a stable agostic isomer was found.

For the CO uptake, **11** → **12**, the incoming CO molecule loses its rotational freedom at a distance of 2.5−3 Å between the carbon atom and the metal center. CO addition leads to charge separation on the CO moiety as well as a transfer of negative charge from the acyl carbon to the Rh atom and the CH_3 group.

We have further shown for the CO uptake reaction that the slow growth dynamics method is able to yield free energies of activation in a very straightforward manner for reactions which do not have an energetic barrier. The barrier found for CO uptake of *trans*-**11** was $\Delta F_N^{\ddagger} = +11$ kJ/mol, whereas the total exothermicity was estimated to be $\Delta F_N = 44$ kJ/mol. This estimate is in good agreement with the ADF result of $\Delta E = -58$ kJ/mol, given the short duration of our molecular dynamics simulation. We have not been as successful in estimating the free energy changes for the other two reactions investigated here in comparison with the ADF estimates. This is understandable since the RC used in the present work often has a very small projection on the true intrinsic reaction coordinate (IRC) at some stage of the process. This leads to rather abrupt releases of energy into specific degrees of freedom, having a detrimental effect on the calculation of free energy.

The barrier to reductive elimination of acetaldehyde to regenerate the catalyst is 50 and 38 kJ/mol for the *trans* and *cis* paths, respectively. The elimination of acetaldehyde from **12** proceeds via a three-centered transition state and results in the immediate formation of the square-planar precatalyst **1**. Elimination removes the polarization of the carbon monoxide ligand and also restores the electron density at the metal center, in accord with the reductive character of the elimination.

Acknowledgment. This work has been supported by the National Sciences and Engineering Research Council of Canada (NSERC), as well as by the donors of the Petroleum Research Fund, administered by the American Chemical Society (ACS-PRF No 20723-AC3). P.M. would like to thank the Austrian Fonds zur Förderung der wissenschaftlichen Forschung (FWF) for financial support within project JO1099-CHE.

JA954168+